

Quantum optical diode with semiconductor microcavities

H. Z. Shen¹, Y. H. Zhou¹, and X. X. Yi^{2*}

¹ *School of Physics and Optoelectronic Technology*

Dalian University of Technology, Dalian 116024, China

² *Center for Quantum Sciences and School of Physics,
Northeast Normal University, Changchun 130024, China*

(Dated: April 4, 2018)

The semiconductor diode, which acts as an electrical rectifier and allows unidirectional electronic transports, is the key to information processing in integrated circuits. Analogously, an optical rectifier (or diode) working at specific target wavelengths has recently become a promising device in optical communication and signal processing. In this paper, we propose a scheme to realize an optical diode for photonic transport at the level of few photons. The system consists of two spatially overlapping single-mode semiconductor microcavities coupled via $\chi^{(2)}$ nonlinearities. The photon blockade is predicted to take place in this system. These photon blockade effects can be achieved by tuning the frequency of the input laser field (driving field). Based on those blockades, we derive analytically the single- and two-photon current in terms of zero and finite-time delayed two-order correlation function. The results suggest that the system can serve as a single- and two-photon quantum optical diodes which allow transmission of photons in one direction much more efficiently than in the other.

PACS numbers: 42.50.-p, 73.40.Ei, 78.66.Fd

Keywords: quantum optical diode, photon conversion, photon blockade

I. INTRODUCTION

The electrical diode is a two-terminal electronic device with asymmetric conductance, it has low resistance to current flow in one direction, and high resistance in the opposite direction. The study on electrical diodes can be traced back to more than one century ago, when the first device enables the rectification of current flux. Motivated by the significant rectifying capabilities of electric diodes, considerable efforts have been made to investigations of the rectification of other energy forms, for example, thermal flux [1–6] and solitary waves [7].

Efforts have also been made for the optical diodes. Optical diodes, also known as optical isolators [8], are an optical rectifier working at specific target wavelengths, they allow propagation of photon signal in one direction and block that in the opposite direction. Motivated by potential applications in quantum network of light, various possible solid-state optical diodes have been proposed, including the diodes from standard bulk Faraday rotators [9, 10], the diodes integrated on a chip [11–15], and diodes operating in optically controllable way [11, 16, 17], as well as the diodes at low field intensities or even at the single-photon levels [18].

The physics behind the optical diode is the breaking of time reversal symmetry, which is typically achieved via acoustic rectifiers [19, 20], moving photonic crystal [21], spin-photon entangling [22] and few-photon tunneling [23–25]. Thanks to the classical level these schemes work at, they have now been attained in different configurations on-chip [14, 26, 27].

With the recent advances in quantum photonic technologies at the single-photon levels [28], researchers make a step further in the study of optical diode—*quantum optical diode*, tunable single- or two-photon quantum rectification is likely to play an important role in this case analogous to the classical electrical diodes in current microchips. A quantum optical rectifier is a two terminal, spatially nonreciprocal device that allows unidirectional propagation of single- or few quanta of (electromagnetic) energy at a fixed signal frequency and amplitude [29]. Up to now, only few proposals have been proposed [18, 29] in fully quantum regime.

In this paper, we propose a fully quantum diode with two coupled semiconductor microcavities driven by external fields. The merit of this proposal is to unify the unidirectional transport of photon and photon conversion. The system consists of two spatially overlapping single-mode cavities with frequencies ω_b and ω_a , respectively. The two cavities are coupled by $\chi^{(2)}$ nonlinearities that mediate the conversion of a photon in cavity b to two photons in cavity a and vice versa [30–34]. The physics behind this proposal is the photon blockade. When cavity a is pumped, single photon blockade prevails in the system, the single photon who occupies the Fock state first blockades the generation

* Corresponding address: yixx@nenu.edu.cn

of more photons. When the pumping is on cavity b , due to the existence of the two-photon eigenstate of the system, two-photon blockade dominates, blocking more photons in cavity b .

The single-photon blockade was already observed in the standard cavity quantum electrodynamics (QED) [35–44], optomechanical systems [45–48] and in circuit QED system [49, 50]. The proposal presented here is to use these techniques and show the single- and two-photon blockade effect by changing the intensity and frequency of the driving field.

The remainder of the paper is organized as follows. In Sec. II, we introduce the system and present a model to describe the system. The single- and two-photon blockade is predicted and discussed. In Sec. III, in terms of the two-order correlation function and photon number statistics, we analyze a specific single-photon and two-photon diode. In Sec. IV, we investigate the rectification of the diode via two-time correlation functions. Discussion and conclusions are given in Sec. V.

II. MODEL AND PHOTON BLOCKADE

Throughout this work, we adopt the International System (SI) of units [51]. The nonlinear optical response of dielectric material to an electric field is given by

$$D_i(\mathbf{r}, t) = \sum_{jkm} \{ \varepsilon_0 \varepsilon_{ij}(\mathbf{r}) E_j(\mathbf{r}, t) + \varepsilon_0 [\chi_{ijk}^{(2)}(\mathbf{r}) E_j(\mathbf{r}, t) \times E_k(\mathbf{r}, t) + \chi_{ijkm}^{(3)}(\mathbf{r}) E_j(\mathbf{r}, t) E_k(\mathbf{r}, t) \times E_m(\mathbf{r}, t) + \dots] \}, \quad (1)$$

which defines the relative dielectric permittivity tensor of the medium, $\varepsilon_{ij}(\mathbf{r}) = \delta_{ij} + \chi_{ij}^{(1)}(\mathbf{r})$. We will consider only the nonlinear response up to second order in the electromagnetic field, i.e., we assume $\chi_{ijkm}^{(3)}(\mathbf{r}) = 0$ and only take the optical nonlinear effects caused by $\chi_{ijk}^{(2)}$ in Eq. (1) into account. We assume the material is isotropic, i.e., $\varepsilon_{ij}(\mathbf{r}) \rightarrow \varepsilon(\mathbf{r})$ is a spatially dependent scalar quantity. The canonical quantization can be done by expressing the field operators as

$$\hat{E}(\mathbf{r}, t) = \sum_{j=a,b} \sqrt{\frac{\hbar\omega_j}{2\varepsilon_0}} [\hat{h}_j \frac{\vec{\phi}_j(\mathbf{r})}{\sqrt{\varepsilon(\mathbf{r})}} e^{-i\omega_j t} + H.c.], \quad (2)$$

and $\hat{B}(\mathbf{r}, t) = -\nabla \times \hat{E}(\mathbf{r}, t)/\omega_0$, with H.c. standing for the Hermitian conjugate. Here $\hat{h}_a = \hat{a}$ and $\hat{h}_b = \hat{b}$ denote the photon destruction operators in the two cavity with frequencies ω_a and $\omega_b = 2\omega_a$, respectively. For each cavity mode, the three-dimensional cavity field $\phi_j(\mathbf{r})$ must be normalized by $\int |\vec{\phi}_j(\mathbf{r})|^2 d^3\mathbf{r} = 1$ ($j=a,b$). By the energy density formula in classical electrodynamics, $H_{em} = \frac{1}{2} \int [\mathbf{E}(\mathbf{r}, t) \cdot \mathbf{D}(\mathbf{r}, t) + \int \mathbf{H}(\mathbf{r}, t) \cdot \mathbf{B}(\mathbf{r}, t)] d^3\mathbf{r}$, where $\mathbf{H}(\mathbf{r}, t) = \mathbf{B}(\mathbf{r}, t)/\mu_0$, an interaction Hamiltonian in the second quantization can be obtained [30, 32]

$$\hat{H}_0 = \hbar\omega_a \hat{a}^\dagger \hat{a} + \hbar\omega_b \hat{b}^\dagger \hat{b} + \hbar\Omega(\hat{b}^\dagger \hat{a}^2 + H.c.) \quad (3)$$

where the nonlinear interaction coefficient is defined by,

$$\Omega = \sqrt{\frac{\hbar^3 \omega_a^2 \omega_b}{8\varepsilon_0}} \sum_{ijk} \int \frac{\chi_{ijk}^{(2)}(\mathbf{r})}{[\varepsilon(\mathbf{r})]^{1.5}} \phi_{i,a}^*(\mathbf{r}) \phi_{j,a}^*(\mathbf{r}) \phi_{k,b}(\mathbf{r}) d^3\mathbf{r}. \quad (4)$$

For the scheme to work, external driving for cavity a or b is essential. We illustrate the setup in Fig. 1 (a), the driving frequency is denoted by ω_L for cavity a and $2\omega_L$ for cavity b , respectively. F stands for the driving strength. The corresponding Hamiltonian is,

$$\hat{H}_{dr}(t) = \hat{H}_0 + \hbar F \hat{h}_j e^{-i\lambda_j \omega_L t} + \hbar F^* \hat{h}_j^\dagger e^{i\lambda_j \omega_L t}, \quad (5)$$

where $\lambda_a = 1$ and $\lambda_b = 2$. In a rotating frame defined by $\hat{U}_S(t) = \exp[i\omega_L t(\hat{a}^\dagger \hat{a} + 2\hat{b}^\dagger \hat{b})]$, the Hamiltonian takes,

$$\hat{H}_S = \hbar\Delta_a \hat{a}^\dagger \hat{a} + \hbar\Delta_b \hat{b}^\dagger \hat{b} + \hbar\Omega(\hat{b}^\dagger \hat{a}^2 + \hat{a}^{\dagger 2} \hat{b}) + \hbar F \hat{h}_j + \hbar F^* \hat{h}_j^\dagger. \quad (6)$$

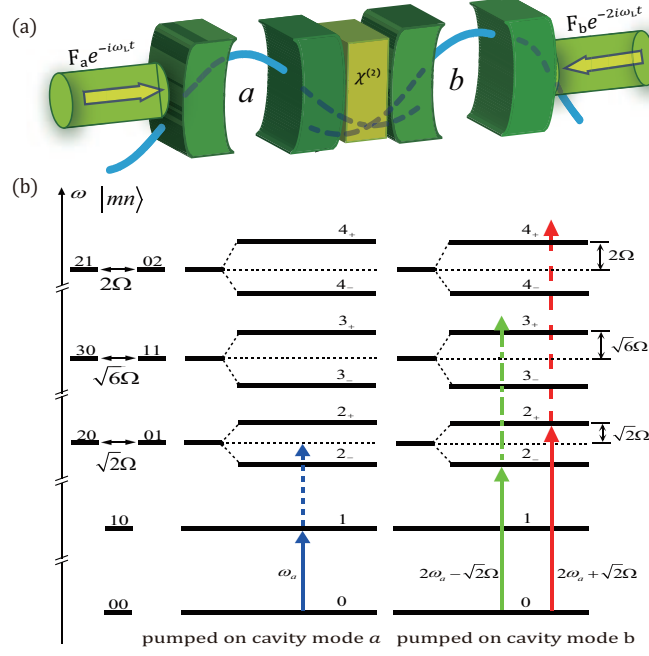


FIG. 1: (Color online) (a) Illustration of the setup. The two cavities driven by external fields (pumping) are coupled by χ^2 nonlinearities. The pumping on the cavity a is resonant with the field inside cavity a , while the pumping on cavity b is at $2\omega_a + \sqrt{2}\Omega$ or $2\omega_a - \sqrt{2}\Omega$. (b) Level diagram for the two coupled cavities with $\omega_b = 2\omega_a$. States are labeled by $|mn\rangle$ with the first(second) number denoting the photon number in cavity a (cavity b). The coupling Ω splits the degeneracy of states $|mn\rangle$ and $|m-2n+1\rangle$ or $|m+2n-1\rangle$. The arrows show the frequency of the driven field.

$\Delta_a = \omega_a - \omega_L$ and $\Delta_b = \omega_b - 2\omega_L$ define the detunings of cavity a and cavity b modes from the driving laser, respectively.

The nonlinear terms proportional to Ω in Eq. (6) describe coherent photon exchange between the two optical cavity modes. The resulting low-energy level diagram is shown in Fig. 1 (b), where $|mn\rangle$ as before represents a state with m and n photons in the cavity a and b , respectively. In the absence of driving fields, we diagonalize \hat{H}_S with $\omega_b = 2\omega_a$ and $\omega_L = \omega_a$. The ground state and low excited state are listed below,

$$\begin{aligned}
 |0\rangle &= |00\rangle, \\
 |1\rangle &= |10\rangle, \\
 |2_{\pm}\rangle &= \frac{1}{\sqrt{2}} |01\rangle \pm |20\rangle, \\
 |3_{\pm}\rangle &= \frac{1}{\sqrt{2}} |11\rangle \pm |30\rangle, \\
 |4_{\pm}\rangle &= \frac{1}{\sqrt{2}} |02\rangle \pm |21\rangle.
 \end{aligned} \tag{7}$$

The driving field couples all states which differ from each other by a single photon. In the following sections, we will restrict ourselves to consider a very weak driving field such that the Hilbert space can be truncated to low energy levels, as listed in Eq. (7).

In addition to the coherent evolution governed by the Hamiltonian \hat{H}_S , we introduce cavity losses to the system, and the dynamics of system is described by,

$$\dot{\rho} = -i[\hat{H}_S, \rho] + \kappa_a \mathcal{D}(\hat{a})\rho + \kappa_b \mathcal{D}(\hat{b})\rho, \tag{8}$$

where \hat{H}_S is given by Eq. (6), κ and κ_a denotes loss rates for the two cavities, respectively, the superoperator $\mathcal{D}(\hat{o}) = \hat{o}\rho\hat{o}^\dagger - \frac{1}{2}\hat{o}^\dagger\hat{o}\rho - \frac{1}{2}\rho\hat{o}^\dagger\hat{o}$. According to the Markovian input-output formalism of Collett and Cardiner [52–54],

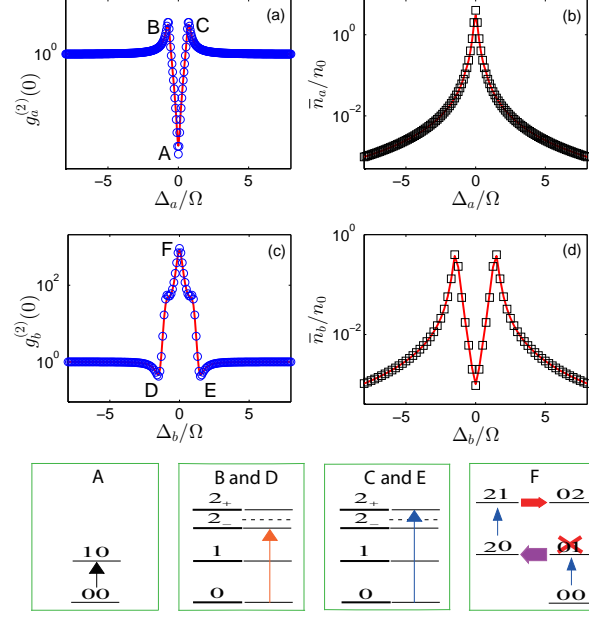


FIG. 2: (color online) **Rescaled average photon number** (black “□”) and the equal-time second-order correlation function (blue “○”) as a function of detunings. *The photon number is rescaled by F^2 to fit the correlation function.* (a) and (b) are for the case with cavity a pumped, and (c) and (d) for cavity b pumped. Once one cavity is pumped, another is left free. Dotted lines are analytical results [see Eqs. (14)-(17)]. Red-solid lines show the numerical results. In all plots, we chose $\Omega/\kappa = 4$, $F/\kappa = 0.2$, $\omega_a/\kappa = 1$, $\omega_b/\kappa = 2$, $\kappa_a/\kappa = 1$. A, B, C, D, E, and F mark the maximum and minimum, the corresponding detunings are, A: $\Delta_a/\Omega = 0$, B: $-\frac{1}{\sqrt{2}}$, C: $\frac{1}{\sqrt{2}}$, D: $\Delta_b/\Omega = -\sqrt{2}$, E: $\sqrt{2}$, and F: 0. The tiny deviation of the analytical results from the numerical ones caused by the approximation $F/\kappa \ll 1$ used in Eqs. (14)-(17). A-F in the bottom panels illustrate the transitions that may lead to the features seen at the points A-F. Suppression of the steady-state population of the level $|01\rangle$ is indicated by a red X. More understanding of the features can be found in the main text.

the input, output, and intracavity fields are linked by the input-output relation,

$$\begin{aligned}\hat{a}_{out}(t) &= \hat{a}_{in}(t) + \sqrt{\kappa_a}\hat{a}(t), \\ \hat{b}_{out}(t) &= \hat{b}_{in}(t) + \sqrt{\kappa_b}\hat{b}(t).\end{aligned}\quad (9)$$

For an arbitrary state of the input modes, correlations of the output fields would depend on cross correlations between the input and intracavity fields, which in turn would require to model the input fields together with the system dynamics. However, if we assume that only classical driving fields is added to the quantum vacuum of the input-output channels, then all normally ordered cross correlations between intracavity and input modes vanish, and correlations in the output channels can be expressed as functions of intracavity correlations only. With this assumption, the average output current (or photon stream) at time t can be formally given by,

$$N_j(t) = \kappa_j Tr[\hat{h}_j^\dagger \hat{h}_j \rho(t)]. \quad (10)$$

We will set $\kappa_b \equiv \kappa$ hereafter.

Now we discuss photon-blockade effect. This effect can be characterized by the second order correlation function with no time-delay [55, 56]

$$g_j^{(2)}(0) = \frac{\langle \hat{h}_j^{\dagger 2} \hat{h}_j^2 \rangle}{\langle \hat{h}_j^\dagger \hat{h}_j \rangle^2}, \quad (11)$$

where all operators are evaluated at the same instance of time. In Fig. 2 we show $g_a^{(2)}(0)$ and $g_b^{(2)}(0)$ as a function of detuning. The figures are plotted in the weak driving limit. Interesting features can be found at detunings $0, -\frac{1}{\sqrt{2}}, \frac{1}{\sqrt{2}}, -\sqrt{2}, \sqrt{2}$, and 0 marked respectively by A, B, C, D, E, and F. Recall that $g_j^{(2)}(0) < 1$ indicates photon

antibunching, and $g_j^{(2)}(0) \rightarrow 0$ implies complete photon blockade, we find that the point A exactly corresponds to the single-photon blockade, similar to that in Kerr-type [36, 55, 57] or QED [35–41] nonlinear systems. Remarkably, when the cavity b is pumped, two-photon blockade for cavity a occurs. This can be found at points D and E in Fig. 2 (c)]. Of course for the cavity b , it is still a single photon blockade. We refer to this effect as the two-photon blockade from the aspect of cavity a , which means that the two-photon Fock states blockade the generation of more photons.

To gain more insights into the single- and two-photon blockade shown in Fig. 2, we develop an approximately analytic expression for the system by considering only the eight lowest energy levels in Fig. 1 (b). Assume that the system is initially prepared in $|00\rangle$, and only these levels are occupied due to the pumping of the driving, the state of the system can be written as, [58]

$$|\Phi\rangle = C_{00}|00\rangle + C_{10}|10\rangle + C_{01}|01\rangle + C_{20}|20\rangle \\ + C_{11}|11\rangle + C_{30}|30\rangle + C_{21}|21\rangle + C_{02}|02\rangle, \quad (12)$$

besides, we take an effective Hamiltonian, $\hat{H}_{eff} = \hat{H}_S - i[\kappa_a \hat{a}^\dagger \hat{a} + \kappa_b \hat{b}^\dagger \hat{b}]/2$ to describe the system. This approach allows us to evaluate the mean occupation numbers up to the order of F^2 and the second-order correlation function up to the order of F^4 . By substituting $|\Phi\rangle$ into the Schrödinger equation $i\partial_t |\Phi\rangle = \hat{H}_{eff} |\Phi\rangle$ ($\hbar = 1$, hereafter), we find the following coupled equations,

$$\begin{aligned} \dot{C}_{00} &= 0, \\ \dot{C}_{10} &= -iFC_{11} - \delta_a C_{10}, \\ \dot{C}_{20} &= -i\sqrt{2}\Omega C_{01} - 2\delta_a C_{20}, \\ \dot{C}_{01} &= -i\sqrt{2}\Omega C_{20} - iFC_{00} - \delta_b C_{01}, \\ \dot{C}_{11} &= -i\sqrt{6}\Omega C_{30} - iFC_{10} - (\delta_a + \delta_b)C_{11}, \\ \dot{C}_{30} &= -i\sqrt{6}\Omega C_{11} - 3\delta_a C_{30}, \\ \dot{C}_{21} &= -i2\Omega C_{02} - iFC_{20} - (2\delta_a + \delta_b)C_{21}, \\ \dot{C}_{02} &= -i2\Omega C_{21} - i\sqrt{2}FC_{01} - 2\delta_b C_{02}, \end{aligned} \quad (13)$$

where $\delta_j = \kappa_j/2 + \Delta_j i$, and the cavity b being pumped was assumed. At steady states, these amplitudes C_{ij} do not evolve, the mean occupation numbers in this case are $\bar{n}_a = 2|\bar{C}_{20}|^2$ and $\bar{n}_b = |\bar{C}_{01}|^2$, where \bar{C}_{ij} denote the amplitude at steady-state. Up to first order in F/κ (see Appendix A), the mean photon number is,

$$\begin{aligned} \frac{\bar{n}_a}{n_0} &= \frac{2\Omega^2}{S\left(\frac{1}{4}, -\Delta_b, 1, \frac{\Delta_b}{2}, \frac{1}{2}\right)}, \\ \frac{\bar{n}_b}{n_0} &= \frac{4S(1, 0, 0, 0, 2)}{S(1, -4\Delta_b, 4, 2\Delta_b, 2)}, \end{aligned} \quad (14)$$

where $S(a, b, c, d, e) = (a\kappa_a + b\Delta_a + c\Omega^2)^2 + (d\kappa_a + e\Delta_a)^2$ and $n_0 = (F/\kappa)^2$. From $S(a, b, c, d, e)$ in these equations, we can obtain the location for local maxima and minima of the average photon numbers, which are in excellent agreement with the numerical results shown in Fig. 2. The eight-level model also provides us with the analytical expression of the second-order correlation functions (see Appendix A),

$$\begin{aligned} g_a^{(2)}(0) &= \frac{S\left(\frac{1}{4}, -\Delta_b, 1, \frac{\Delta_b}{2}, \frac{1}{2}\right)}{4F^2\Omega^2}, \\ g_b^{(2)}(0) &= \frac{S\left(-\frac{1}{2}a_0, 2\Delta_a + \Delta_b, 1, 2\Delta_a + \frac{1}{2}\Delta_b, \frac{1}{2}\right)}{S\left(-\frac{1}{2}, 2\Delta_b, -2 + \frac{-1+4\Delta_b^2}{4\Omega^2}, \Delta_b, 1 + \frac{\Delta_b}{\Delta_a}\right)} \\ &\quad \cdot \frac{S(1, -4\Delta_b, 4, 2\Delta_b, 2)}{S^2(1, 0, 0, 0, 2)}, \end{aligned} \quad (15)$$

where $a_0 = \kappa_a + 1/2$. By the same approach, we can obtain the following equations for the case of cavity a being

pumped,

$$\begin{aligned}
\dot{C}_{00} &= 0, \\
\dot{C}_{10} &= -iFC_{00} - i\sqrt{2}FC_{20} - \delta_a C_{10}, \\
\dot{C}_{20} &= -i\sqrt{2}\Omega C_{01} - 2\delta_a C_{20} - i\sqrt{2}FC_{10}, \\
\dot{C}_{01} &= -i\sqrt{2}\Omega C_{20} - \delta_b C_{01}, \\
\dot{C}_{11} &= -i\sqrt{6}\Omega C_{30} - iFC_{01} - i\sqrt{2}FC_{21} \\
&\quad - (\delta_a + \delta_b)C_{11}, \\
\dot{C}_{30} &= -i\sqrt{6}\Omega C_{11} - 3\delta_a C_{30} - i\sqrt{3}FC_{20}, \\
\dot{C}_{21} &= -i2\Omega C_{02} - i\sqrt{2}FC_{11} - (2\delta_a + \delta_b)C_{21}, \\
\dot{C}_{02} &= -i2\Omega C_{21} - 2\delta_b C_{02}.
\end{aligned} \tag{16}$$

The steady-state amplitudes (see Appendix A) are given by,

$$\begin{aligned}
\frac{\bar{n}_a}{n_0} &= \frac{4}{S(1, 0, 0, 0, 2)}, \\
\frac{\bar{n}_b}{n_0} &= \frac{(F\Omega)^2}{S\left(\frac{1}{2}, 0, 0, 0, 1\right) \cdot S\left(\frac{1}{4}, -\Delta_b, 1, \frac{\Delta_b}{2}, \frac{1}{2}\right)}, \\
g_a^{(2)}(0) &= \frac{S(1, 0, 0, 0, 2) \cdot S\left(\frac{1}{\kappa_a}, 0, 0, \frac{2\Delta_b}{\kappa_a}, 0\right)}{S(1, -4\Delta_b, 4, 2\Delta_b, 2)}, \\
g_b^{(2)}(0) &= \frac{S(1, 0, 0, 0, 2) \cdot S\left(\frac{1}{4}, -\Delta_b, 1, \frac{\Delta_b}{2}, \frac{1}{2}\right)}{S(a_1, b_1, c_1, d_1, e_1) \cdot S^{-1}\left(\frac{\Delta_b}{\kappa_a}, 1, 0, \frac{1}{2}, \frac{1}{2\Delta_a}\right)},
\end{aligned} \tag{17}$$

where,

$$\begin{aligned}
a_1 &= -\frac{1}{16} - \frac{3\kappa_a}{16} - \frac{\kappa_a^2}{8} + \frac{3\Delta_b^2}{4} + \frac{3\kappa_a\Delta_b^2}{4}, \\
b_1 &= \frac{3\Delta_a}{4} + \frac{3\kappa_a\Delta_a}{2} - 3\Delta_a\Delta_b^2 - \Delta_b^3 + \Delta_b f_1, \\
c_1 &= -\frac{1}{2} - \frac{3\kappa_a}{2} - \frac{\kappa_a^2}{2} + 2\Delta_a^2 + 2\Delta_b^2 - 4\Omega^2, \\
d_1 &= -\frac{3\Delta_a}{4} - 3\Delta_b\Omega^2 - \frac{3}{4}\kappa_a\Delta_a + \frac{\Delta_b^3}{2} + \Delta_b g_1, \\
e_1 &= -\frac{1}{8} + \Delta_a^2 + 3\Delta_a\Delta_b + \frac{3}{2}\Delta_b^2 + \Omega^2 h_1.
\end{aligned} \tag{18}$$

Here, $f_1 = \frac{3}{4} + 3\kappa_a + \frac{3\kappa_a^2}{2} - 2\Delta_a^2 + 6\Omega^2$, $g_1 = -\frac{3}{8} - \frac{3}{4}\kappa_a - \frac{1}{4}\kappa_a^2 + 3\Delta_a^2 + 3\Delta_a\Delta_b$, $h_1 = -3 - 2\frac{\Delta_b}{\Delta_a} - 2\kappa_a$. Similarly, by analyzing $S(a, b, c, d, e)$ in Eqs. (14)-(17), we can obtain interesting points in $g_{a,b}^{(2)}(0)$ labeled by A, B, C, D, E, and F, which are in excellent agreement with the numerical results shown in Fig. 2.

We now discuss the features observed in Fig. 2. We will use the eight-level model together with the diagonal basis in Eq. (7) to understand the physics behind the features. In (a) and (b), i.e., the pumping is on microcavity a , when the detuning is zero, $\Delta_a = 0$ (point A in Fig. 2), we can see $g_a^{(2)}(0) \ll 1$, indicating complete antibunching due to the suppressed two-photon process (panel A in Fig. 2), this leads to the single-photon blockade. Physically, when the left cavity a is pumped by a incident laser of frequency ω_L , a incident photon with the the same frequency as the cavity field ω_a will excite the cavity from vacuum $|0\rangle$ to the first excited state $|1\rangle$ [marked by the blue-dotted arrow in Fig. 1 (b)]. Once the cavity has a photon, the second photon at that frequency will be blocked because, due to the nonlinearity of (3), excitation of the system from $|1\rangle$ to $|2_+\rangle$ or $|2_-\rangle$ requires an additional energy $\hbar\sqrt{2}\Omega$, which cannot be supplied by the second photon. At the detuning $\Delta_a/g = \pm\frac{1}{\sqrt{2}}$ (point B and C of (a)), bunching happens due to the two-photon resonant transition $|0\rangle \rightarrow |2_+\rangle$ and $|2_-\rangle$ (panel B and C), the physics behind this bunching is similar.

A similar story takes place when the microcavity b is pumped, see Fig. 2 (c). At detuning $\Delta_b/g = \pm\sqrt{2}$ (point D and E of (c)), resonant transition $|0\rangle \rightarrow |2_+\rangle$ and $|2_-\rangle$ (panel D and E) occurs, indicating almost completely

antibunching for cavity mode b . Mathematically, we find that both the single-photon occupation amplitude \bar{C}_{10} , the three-photon occupation amplitude \bar{C}_{11} and \bar{C}_{30} equals to zero, while the two-photon occupation amplitude \bar{C}_{01} and \bar{C}_{20} are much larger than that of four-photon under the weak driving limit $|\alpha_j \alpha_k| \ll 1$, see Eq. (A1). The point F in Fig. 2 corresponds to detuning $\Delta_b = 0$. $g_b^{(2)}(0) \gg 1$ at this point, indicating strong bunching. This is due to destructive interference that suppresses the population on $|01\rangle$ (panel F in Fig. 2), steering the system into a dark state, $|dark\rangle = -\cos\varphi|00\rangle + \sin\varphi|20\rangle$, where $\tan\varphi = F/\Omega$. This is reminiscent of the electromagnetically induced transparency [59, 60]. Due to the weak coupling, $|20\rangle$ is almost not populated when the system occupies the dark state, this induces the transition from $|20\rangle$ to $|21\rangle$, which in turn is strongly coupled to $|02\rangle$. The net result is the transition with one photon is suppressed compared to the two-photon transition, leading to the bunching at $\Delta_b = 0$.

To confirm this point, we now show that two-photon resonance is absent at $\Delta_b = 0$. At first glance, the level diagram in Fig. 1(b) together with bunching at point F in Fig. 2 suggest a two-photon resonance at zero detuning $\Delta_b = 0$, where the energy of the two-photon state $|02\rangle$ is equal to the energy of two incident photons in mode b . However, as discussed above, the strong bunching effect at $\Delta_b = 0$ comes completely from the suppression of the one-photon population. Further, we find that the expected two-photon resonance is canceled by interference. This can be seen from a second-order perturbative calculation of the two-photon Rabi frequency $\omega_{00 \rightarrow 02}^{(2)}$ for the transition $|00\rangle \rightarrow |02\rangle$. The two-photon state $|02\rangle$ can be populated by the drive $\hat{h}_{dr} = F(\hat{b} + \hat{b}^\dagger)$ from vacuum via two intermediate one-photon eigenstates $|2_\pm\rangle$ given by Eq. (7) with energies $\omega_{2\pm} = \Delta_b \pm \sqrt{2}\Omega$ in the rotating frame. The resulting Rabi frequency is

$$\omega_{00 \rightarrow 02}^{(2)} = \sum_{m=2_+, 2_-} \langle 20 | \hat{h}_{dr} | m \rangle \langle m | \hat{h}_{dr} | 00 \rangle / \omega_m, \quad (19)$$

which vanishes at $\Delta_b = 0$ as a consequence of destructive interference between the two amplitudes. Although the exact cancelation is lifted by including finite dissipation and the full spectrum, this simple argument shows that the expected two-photon resonance at $\Delta_b = 0$ is strongly suppressed.

It is important to address that the photon blockade in the case of cavity b being driven is a two-photon blockade from the side of cavity a , hence we refer to this type of photon blockade as two-photon blockade.

So far, we have demonstrated both analytically and numerically a variety of quantum properties revealing the unique nature of the single- and two-photon blockade. The results suggest that by manipulating the detuning, optical diodes may be realized in such a system based on the explicit single- and two-photon blockade.

III. SINGLE-PHOTON AND TWO-PHOTON DIODE

By the use of the blockade features of the photonic semiconductor microcavities and the χ^2 nonlinearities, in this section we present a scheme to realize a single-photon and two-photon diode. We define a rectifying factor as the normalized difference between the two output currents corresponding to the system being pumped through the left and right cavities (indicated by the wave vectors k and $-k$, respectively) [29]

$$R = \frac{2N_b(k) - N_a[-k]}{2N_b(k) + N_a[-k]}. \quad (20)$$

Substituting Eqs. (14)-(17) into Eq. (20), we can obtain an analytical expression of the rectifying factor,

$$R = \frac{\kappa F^2 - \kappa_a S[\frac{1}{2}, 0, 0, 0, 1]}{\kappa F^2 + \kappa_a S[\frac{1}{2}, 0, 0, 0, 1]}. \quad (21)$$

By this definition, $R = -1$ implies maximal rectification with enhanced transport to the left (left rectification), $R = 0$ indicates no rectification, while $R = 1$ describes maximal rectification with transport to the right (right rectification).

In Fig. 3, we plot the second-order correlation function of the left cavity a [see (a)] and right cavity b [see (b)] when the system is pumped on the cavity a . We find that the normalized correlations of $g_j^{(2)}(0) \ll 1$ reach their minimum at $\Delta = 30\kappa$ (namely, $\Delta_a \approx 0$), implying the well known single photon blockade. The diagram (c) in Fig. 3 illustrates the transition for this blockade.

In Fig. 4, we plot the correlation function of cavity a [see (a)] and cavity b [see (b)] when the system is pumped on the right cavity b . We observe that the minimum of $g_b^{(2)}(0)$ is on an ellipse defined by Eq. (22) and shown in Fig. 4 (c). This can be explained as the condition for the two-photon blockade to happen in the system, i.e., two photon resonance $2\omega_L = \omega_{2\pm}$ follows

$$\Delta^2 + 8\Omega^2 = x^2, \quad (22)$$

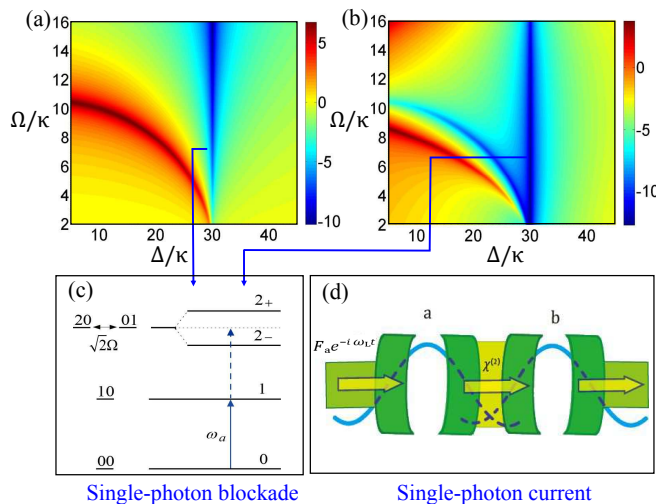


FIG. 3: (Color online) Single-photon rectification in the semiconductor microcavities coupled via χ^2 nonlinearities. The equal-time second-order correlation function when the system is pumped on the cavity a [see analytical expression Eq. (17)] (log scale). (a) is for the cavity a and (b) for the cavity b . We set $x = \Delta_b + 2\Delta_a$, with detunings given by $\Delta = \Delta_b - 2\Delta_a$ corresponding to $\Delta_a = (x - \Delta)/4$ and $\Delta_b = (x + \Delta)/2$. Parameters chosen are $\kappa_a = 0.1\kappa$, $F = 0.1\kappa$, $\Omega = 10\kappa$, $x = 30\kappa$. The very narrow region around $\Delta = 30\kappa$, i.e., $\Delta_a \approx 0$, shows the complete single-photon blockade, the corresponding transition is shown in Fig. 3-(c), and the single-photon current to right cavity b is illustrated in (d).

where $x = \Delta_b + 2\Delta_a$ and $\Delta = \Delta_b - 2\Delta_a$. Analogously, the bunching of a pair of photons for the left cavity a take place due to the extreme antibunching of the right cavity b .

Fig. 5 shows R , $g^{(2)}$ and N as a function of laser frequency with a fixed Δ in the small Ω/κ limit. We find a local maximum of left rectification in Fig. 5 (a) at $x = 30\kappa$ (marked by B in (c)), which corresponds to the anti-bunching in Fig. 5 (b) at the left cavity a . The total photon current $N(k) = N_a(k) + N_b(k)$ overcomes $N(-k)$ in the area around the $x = 30$, see Fig. 5 (c). This can be explained as the single-photon blockade. From Eq. (A4) we can find the single-photon occupation amplitude \bar{C}_{10} is sufficiently larger than that of multiphoton, e.g., two-photon occupation amplitude \bar{C}_{01} and \bar{C}_{20} in the limit of weak optical driving, i.e., $|\alpha_j \alpha_k| \ll 1$.

Two maxima of left rectification can be observed at $x = \pm 10\sqrt{17}\kappa \approx \pm 41.231\kappa$ (marked by A and C) from Fig. 5 due to the two-photon blockade at the ellipse Eq. (22), which corresponds to anti-bunched effect in Fig. 5 (b) at the right cavity b with cavity b pumped (denoted by $-k$). The total photon current $N(-k)$ overcomes $N(k)$ in the area around the two points A and C in Fig. 5 (c). This observation can be explained by examining Eq. (A1), the contribution of the four-photon terms \bar{C}_{21} and \bar{C}_{02} can be neglected compared to the two-photon occupation amplitude \bar{C}_{20} \bar{C}_{01} when the weak optical driving condition $|\alpha_j \alpha_k| \ll 1$, is satisfied. The single-photon occupation amplitude \bar{C}_{10} and three-photon occupation amplitude \bar{C}_{11} and \bar{C}_{30} are equal to zero. Therefore the single- and three-photon processes have no contribution to the two-photon diode.

IV. DELAYED CORRELATION FUNCTION

In addition to the equal-time second-order correlation functions discussed above, quantum signatures can also be manifested in photon intensity correlations with a finite time delay. This motivates us to investigate the dynamical evolution of the second-order time-delayed correlation function. The two-time intensity correlations are defined by [43, 55, 61],

$$g_a^2(\tau) = g_a^2(\tau = t_1 - t, t \rightarrow \infty) = \frac{\langle \hat{a}^\dagger(t) \hat{a}^\dagger(t_1) \hat{a}(t_1) \hat{a}(t) \rangle}{\langle \hat{a}^\dagger(t) \hat{a}(t) \rangle^2}. \quad (23)$$

Rewriting this correlation in terms of a classical light photon intensity I , $g^2(\tau) = \langle I(\tau)I(0) \rangle / \langle I \rangle^2$ and using the Schwarz inequality, we obtain the inequality [37, 58]

$$g^2(\tau) \leq g^2(0). \quad (24)$$

Similar to the inequality $g^{(2)}(0) > 1$ at zero time-delay, violation of the inequality at finite delay is a signature of

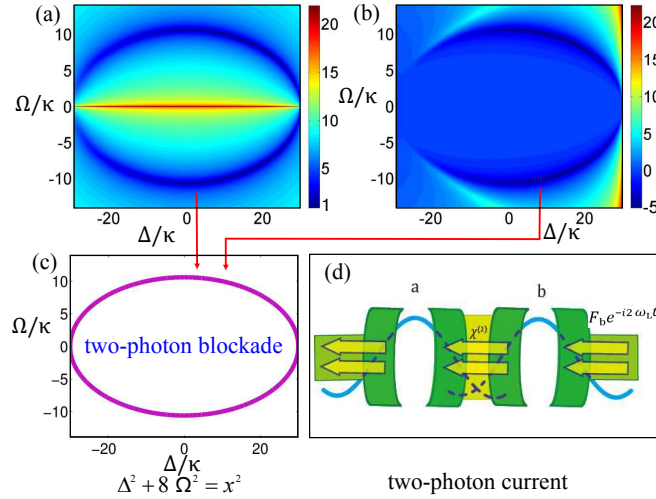


FIG. 4: (Color online) Two-photon rectification in the semiconductor microcavities coupled by χ^2 nonlinearities. The equal-time second-order correlation function [see analytical expression Eq. (15), log scale] of the cavity a (see, (a)) and of the cavity b (see, (b)), this figure is plotted with the right cavity b pumped. We set $x = \Delta_b + 2\Delta_a$ with detunings defined by $\Delta = \Delta_b - 2\Delta_a$. Parameters chosen are $\kappa_a = 0.1\kappa$, $F = 0.1\kappa$, $\Omega = 10\kappa$, $x = 30\kappa$. At the ellipse $\Delta^2 + 8\Omega^2 = x^2$, i.e., two-photon resonant transition from $|0\rangle \rightarrow |2_{\pm}\rangle$ when $2\omega_L = \omega_{2\pm}$, two-photon blockade happens in the semiconductor microcavities, the corresponding transition is illustrated in Fig. 4(c), this causes the two-photon current to the left cavity mode a , see (d). Note that the two-photon current is symmetric for the symmetric coupling Ω in (a) and (b), this is a direct reflection of Eq. (15).

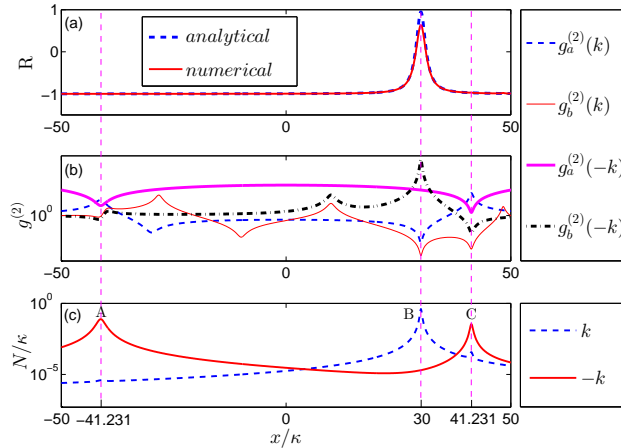


FIG. 5: (Color online) (a) The rectifying factor, correlation function and total current as a function of frequency of the external laser field x . The blue-dashed line and red-bold line denote the rectification factor for the analytical expression Eq. (21) and the fully numerical simulation in (a), respectively. In (b), the equal-time second-order correlation function $g^{(2)}$ [see analytical expression Eqs. (14)-(17)] of the output photon in both directions. (c) shows the total current, $N(k) = N_a(k) + N_b(k)$ [see analytical expression Eqs. (14)-(17)]. Parameters chosen are $\kappa_a = 0.1\kappa$, $F = 0.1\kappa$, $\Omega = 10\kappa$. We assume that $\Delta = 30\kappa$ with $\Delta_a = (x - \Delta)/4$ and $\Delta_b = (x + \Delta)/2$.

quantum nature. We calculate the delayed second-order correlation functions for both the left cavity a and right cavity b when the system is pumped on the left cavity a .

The correlation function $g_a^{(2)}(\tau)$ and $g_b^{(2)}(\tau)$ are shown in Fig. 6 for two strengths of the driving F . We can understand the finite delay intensity correlations in terms of the simple eight-level model discussed in the previous section. For this purpose, we rewrite Eq. (23) as

$$g_a^2(t_1 - t) = \frac{\text{Tr}_S \text{Tr}_E [\hat{a}^\dagger \hat{a} U^\dagger(t - t_1) \hat{\rho}_{\text{tot}}(t) \hat{a} U(t - t_1)]}{\langle \hat{a}^\dagger(t) \hat{a}(t) \rangle^2} \quad (25)$$

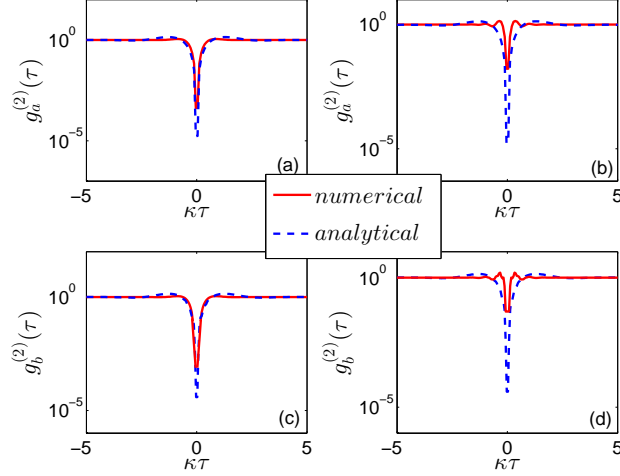


FIG. 6: (Color online) Finite temporal evolution of the second-order correlation function for selected driving strength F with cavity a being pumped. The blue-dashed line and red-bold line denote the analytical expression [given by Eq. (30) and (31)] and the exact numerical simulation, respectively. Parameters chosen are $\kappa_a = 4\kappa$, $F = 1.8\kappa$, $\Omega = 25\kappa$, $\Delta_a = 1.2\kappa$, $\Delta_b = 1\kappa$ for (a) and (c), and $F = 5\kappa$ for (b) and (d).

where the unitary evolution operator $U(t) = \exp(-i\hat{H}_T t)$, $\hat{H}_T = \hat{H}_S + \hat{H}_E + \hat{H}_I$, and \hat{H}_S is given by Eq. (6). \hat{H}_E and \hat{H}_I are the Hamiltonians of the environment and the system-environment interaction, respectively. We assume $\tau = t_1 - t$ and $t \rightarrow \infty$, when the system density matrix arrive at a steady state ρ_s . Applying the Born approximation, we have

$$g_a^2(\tau) = \frac{\text{Tr}_S \text{Tr}_E [\hat{a}^\dagger \hat{a} U(\tau) \hat{a} \rho_s \hat{a}^\dagger \otimes \rho_E U^\dagger(\tau)]}{\bar{n}_a^2}. \quad (26)$$

A simple calculation follows,

$$g_a^2(\tau) = \text{Tr}_S [\hat{A}^\dagger \hat{A} \rho_{new}(\tau)], \quad (27)$$

where

$$\rho_{new}(\tau) = \text{Tr}_E [U(\tau) \rho_{new}(0) \otimes \rho_E U^\dagger(\tau)], \quad (28)$$

where the new initial state is defined by $\rho_{new}(0) = \hat{a} \rho_s \hat{a}^\dagger$ and $\hat{A} = \hat{a} / \bar{n}_a$. From Eq. (27), we can find that the finite delayed second-order correlation function can be thought of as an expectation values of the effective photon number $\hat{A}^\dagger \hat{A}$ with a new density matrix given by Eq. (28). Note that the new dynamical equation is the same as Eq. (8), i.e., $\dot{\rho}_{new}(t) \equiv \dot{\rho}(t)$, except that the new initial condition $\rho(0)$ is replaced by $\rho_{new}(0)$.

Writing the system steady state as $\rho_s = |\bar{\Phi}\rangle \langle \bar{\Phi}|$ and the new time-evolved density matrix as $\rho_{new}(t) = |\Phi_{new}(t)\rangle \langle \Phi_{new}(t)|$, we find $|\dot{\Phi}_{new}(t)\rangle \equiv |\dot{\Phi}(t)\rangle$ satisfying Eq. (16) within the non-Hermitian Hamiltonian approximation. Therefore the time-delayed correlation function can be calculated by introducing a new initial state

$$|\Phi_{new}(0)\rangle = \hat{a} |\bar{\Phi}\rangle, \quad (29)$$

with $|\bar{\Phi}\rangle$ given by Eq. (16) (see Appendix B). With this initial state, we have the time-delayed correlation function,

$$g_a^2(\tau) = \frac{|C_{10}(\tau)|^2}{|\bar{C}_{10}|^4} \quad (30)$$

for the left cavity a , while for the right cavity b ,

$$g_b^2(\tau) = \frac{|C_{01}(\tau)|^2}{|\bar{C}_{01}|^4}, \quad (31)$$

We note the the non-Hermitian Hamiltonian approximation is a good approximation when

$$\Omega^2 \gg \kappa_a \kappa F. \quad (32)$$

We find from Fig. 6 that, when the strong coupling conditions (32) are satisfied [see Figs. 6 (a) and (c)] and the cavity a is pumped, the finite delayed second-order correlation functions given by the analytical expression Eqs. (30) and (31) are in good agreement with those by numerical simulations. When the driving strength is strong (32) [see Figs. 6 (b) and (d)], the analytical expression Eqs. (30) and (31) deviates from the numerical simulations. In addition, from Fig. 6, we can observe that the $g_a^{(2)}(\tau)$ and $g_b^{(2)}(\tau)$ increase above its initial value at finite delay. This is an violation of the inequality in Eq. (24), indicating that photons emitted at different times prefer to stay together. See the red-bold line around $\tau \approx \pm 0.327/\kappa$, in Fig. 6(b) and (d).

This tells that two subsequent emissions are suppressed in single-photon diode, leading to dynamical anti-bunching both for zero- and finite-time delay. Hence our proposal provides us with new insight on the necessary time delay in a single-photon diode in the semiconductor microcavities coupled via $\chi^{(2)}$ nonlinearities.

V. CONCLUSION

In summary, we have presented a scheme for creating an optical diode, the diode is composed of two microcavities coupled via $\chi^{(2)}$ nonlinearities. A master equation to describe such a system is given. By Solving this master equation, single- and two photon blockades are predicted. By the use of this photon blockade, we design an optical diode, which has a merit to combine photon rectification and single photon to two-photon conversion. To characterize the rectification, we calculated both analytically and numerically the two-order correlation function and the rectifying factor in the weakly driven limit. The numerical simulation and analytical expression agree well with each other.

ACKNOWLEDGMENTS

We would like to thank Prof. W. T. M. Irvine for helpful discussions. This work is supported by the NSF of China under Grant No. 11175032.

Appendix A: Analytical expression

In this Appendix, we provide the analytical expression used to calculate zero and finite delayed second-order correlation functions in the steady state. First, zero delayed correlations are calculated by the use of steady-state solutions of Eq. (13). We set the time derivatives to zero and solve the equations iteratively, order by order, in the weak driving. With the right microcavity b being pumped, simple calculation yields

$$\begin{aligned} \bar{C}_{00} &= 1, \bar{C}_{10} = C_{11} = C_{30} = 0, \\ \bar{C}_{20} &= \frac{\alpha_a x_b}{\sqrt{2}(1 - x_a x_b)}, \\ \bar{C}_{01} &= -\frac{\alpha_b}{1 - x_a x_b}, \\ \bar{C}_{21} &= \frac{-\alpha_a \alpha_b (2 + y) x_b}{\sqrt{2}(2 + y - 2x_a x_b)(1 - x_a x_b)}, \\ \bar{C}_{02} &= \frac{\alpha_a \alpha_b (2 + y + x_a x_b y)}{\sqrt{2}y(2 + y - 2x_a x_b)(1 - 2x_a x_b)}, \end{aligned} \quad (A1)$$

where $\alpha_j = -iF/\delta_j(|\alpha_j|^2$ or $|\alpha_j \alpha_k| \ll 1)$, $x_j = -i\Omega/\delta_j$, and $y = \delta_b/\delta_a$. Using these amplitudes, we can express all equal-time averages. The mean photon number is,

$$\begin{aligned} \bar{n}_a &= 2|\bar{C}_{20}|^2, \\ \bar{n}_b &= |\bar{C}_{01}|^2, \end{aligned} \quad (A2)$$

and the photon-photon correlation functions are

$$\begin{aligned} g_b^{(2)}(0) &= \frac{2|\bar{C}_{02}|^2}{|\bar{C}_{01}|^4}, \\ g_a^{(2)}(0) &= \frac{1}{2|\bar{C}_{20}|^2}. \end{aligned} \quad (\text{A3})$$

Therefore Eqs. (14) and (15) can be obtained by substituting Eq. (A1) into Eqs. (A2) and (A3), respectively. Next we calculate these occupation amplitudes for pumping is on the left cavity a ,

$$\begin{aligned} \bar{C}_{00} &= 1, \bar{C}_{10} = -\alpha_a, \\ \bar{C}_{01} &= \frac{\alpha_a \alpha_b x_a}{(x_a x_b - 1)}, \\ \bar{C}_{20} &= -\frac{\alpha_a^2}{\sqrt{2}(x_a x_b - 1)}, \\ \bar{C}_{30} &= \frac{\alpha_a^2 \alpha_b (2 + 3y + y^2 + 2x_a x_b - 4x_a^2 x_b^2)}{\sqrt{6}\lambda(x_a x_b - 1)}, \\ \bar{C}_{11} &= \frac{-\alpha_a \alpha_b^2 x_a (2 + 3y + y^2 - 2x_a x_b - 2x_a^2)}{\lambda(x_a x_b - 1)}, \\ \bar{C}_{21} &= \frac{\sqrt{2}\alpha_a^2 \alpha_b^2 x_a (1 + y)}{\lambda(x_a x_b - 1)}, \\ \bar{C}_{02} &= \frac{-\sqrt{2}\alpha_a^2 \alpha_b^2 x_a x_b (1 + y)}{\lambda(x_a x_b - 1)}, \end{aligned} \quad (\text{A4})$$

where the coefficient $\lambda = (2y^{-1} + 3 + y - 2x_b^2 - 6x_a x_b - 2x_a^2 + 4x_a^2 x_b^2)$. The mean photon numbers and the photon-photon correlation functions are

$$\begin{aligned} \bar{n}_b &= |\bar{C}_{01}|^2, \\ \bar{n}_a &= |\bar{C}_{10}|^2, \\ g_b^{(2)}(0) &= \frac{2|\bar{C}_{02}|^2}{|\bar{C}_{01}|^4}, \\ g_a^{(2)}(0) &= \frac{2|\bar{C}_{20}|^2}{|\bar{C}_{10}|^4}. \end{aligned} \quad (\text{A5})$$

Eq. (17) can be obtained by substituting Eq. (A4) into Eqs. (A5).

Appendix B: delayed correlation function

The dynamical evolution of the second-order correlation function can be calculated within the same approach as in Appendix A. By the use of Eq. (29) as the initial condition and consider a pumping is on the left cavity a . Specifically, the unnormalized state after the annihilation of a photon in the left cavity a is $a|\bar{\Phi}\rangle = \bar{C}_{10}|00\rangle + \sqrt{2}\bar{C}_{20}|10\rangle$, where we have ignored the high-order terms. With this understanding in mind, Eq. (30) can be obtained by solving the first four equations of Eq. (16) for the amplitudes with the initial condition.

The correlation function of the right cavity b mode $g_b^2(\tau)$ may be calculated similarly. The state after annihilation of a photon in the b mode is $b|\bar{\Phi}\rangle = \bar{C}_{01}|00\rangle + \bar{C}_{11}|10\rangle + \bar{C}_{21}|20\rangle + \sqrt{2}\bar{C}_{02}|01\rangle$. Using this as the initial condition, Eq. (31) can be obtained by solving Eq. (16).

[1] B.-W. Li, L. Wang, and G. Casati, Phys. Rev. Lett. **93**, 184301 (2004).

[2] B.-W. Li, J.-H. Lan, and L. Wang, Phys. Rev. Lett. **95**, 104302 (2005).

- [3] C. W. Chang, D. Okawa, A. Majumdar, and A. Zettl, *science* **314**, 1121 (2006).
- [4] W. Kobayashi, Y. Teraoka, and I. Terasaki, *Appl. Phys. Lett.* **95**, 171905 (2009).
- [5] M. Terraneo, M. Peyrard, and G. Casati, *Phys. Rev. Lett.* **88**, 094302 (2002).
- [6] R. Scheibner, M. König, D. Reuter, A. D. Wieck, C. Gould, H. Buhmann, and L. W. Molenkamp, *New J. Phys.* **10**, 083016 (2008).
- [7] V. F. Nesterenko, C. Daraio, E. B. Herbold, and S. Jin, *Phys. Rev. Lett.* **95**, 158702 (2005).
- [8] L. J. Aplet and J. W. Carson, *Appl. Opt.* **3**, 544 (1964).
- [9] P. Yeh, *Optical Waves in Layered Media* (John Wiley and Sons, New York, 1988).
- [10] B. E. A. Saleh and M. C. Teich, *Fundamentals of Photonics* (John Wiley and Sons, New York, 2007), 2nd ed.
- [11] M. S. Kang, A. Butsch, and P. S. Russell, *Nat. Photonics* **5**, 549 (2011)
- [12] A. Kamal, J. Clarke, and M. H. Devoret, *Nat. Phys.* **7**, 311 (2011).
- [13] L. Fan, J. Wang, L. T. Varghese, H. Shen, B. Niu, Y. Xuan, A. M. Weiner, and M.-H. Qi, *Science* **335**, 447 (2012).
- [14] L. Bi, J. Hu, P. Jiang, D. H. Kim, G. F. Dionne, L. C. Kimerling, and C. A. Ross, *Nat. Photonics* **5**, 758 (2011).
- [15] Z. F. Yu and S. H. Fan, *Nat. Photonics* **3**, 91 (2009).
- [16] A. Alberucci and G. Assanto, *Opt. Lett.* **33**, 1641 (2008).
- [17] F. Biancalana, *J. Appl. Phys.* **104**, 093113 (2008).
- [18] Y. Shen, M. Bradford, and J.-T. Shen, *Phys. Rev. Lett.* **107**, 173902 (2011).
- [19] B. Liang, B. Yuan, and J. C. Cheng, *Phys. Rev. Lett.* **103**, 104301 (2009).
- [20] B. Liang, X.-S. Guo, J. Tu, D. Zhang, and J. C. Cheng, *Nat. Materials* **9**, 989 (2010).
- [21] D.-W. Wang, H.-T. Zhou, M.-J. Guo, J.-X. Zhang, J. Evers, and S.-Y. Zhu, *Phys. Rev. Lett.* **110**, 093901 (2013).
- [22] C. Flindt, A. S. Sørensen, M. D. Lukin, and J. M. Taylor, *Phys. Rev. Lett.* **98**, 240501 (2007).
- [23] D. Roy, *Phys. Rev. B* **81**, 155117 (2010).
- [24] G. Nikoghosyan and M. Fleischhauer, *Phys. Rev. Lett.* **103**, 163603 (2009).
- [25] J. C. Blakesley, P. See, A. J. Shields, B. E. Kardynal, P. Atkinson, I. Farrer, and D. A. Ritchie, *Phys. Rev. Lett.* **94**, 067401 (2005).
- [26] L. Fan, J. Wang, L.-T. Varghese, H. Shen, B. Niu, Y. Xuan, A. M. Weiner, and M. Qi, *Science* **335**, 447 (2012).
- [27] H. Lira, Z. Yu, S. Fan, and M. Lipson, *Phys. Rev. Lett.* **109**, 033901 (2012).
- [28] J. L. O'Brien, A. Furusawa, and J. Vučković, *Nat. Photonics* **3**, 687 (2009).
- [29] E. Mascarenhas, D. Valente, S. Montangero, A. Auffèves, D. Gerace, and M. F. Santos, e-print arXiv:1307.6493 (2013).
- [30] W. T. M. Irvine, K. Hennessy, and D. Bouwmeester, *Phys. Rev. Lett.* **96**, 057405 (2006).
- [31] G. S. Agarwal, *Phys. Rev. Lett.* **73**, 522 (1994).
- [32] I. Carusotto and G. C. La Rocca, *Phys. Rev. B* **60**, 4907 (1999).
- [33] A. Majumdar and D. Gerace, *Phys. Rev. B* **87**, 235319 (2013).
- [34] Y.-C. Liu, Y.-F. Xiao, Y.-L. Chen, X.-C. Yu, and Q.-H. Gong, *Phys. Rev. Lett.* **111**, 083601 (2013).
- [35] L. Tian and H. J. Carmichael, *Phys. Rev. A* **46**, R6801 (1992).
- [36] M. J. Werner and A. Imamoğlu, *Phys. Rev. A* **61**, 011801(R) (1999).
- [37] R. J. Brecha, P. R. Rice, and M. Xiao, *Phys. Rev. A* **59**, 2392 (1999).
- [38] S. Rebić, S. M. Tan, A. S. Parkins, and D. F. Walls, *J. Opt. B* **1**, 490 (1999).
- [39] S. Rebić, A. S. Parkins, and S. M. Tan, *Phys. Rev. A* **65**, 063804 (2002).
- [40] J. Kim, O. Bensen, H. Kan, and Y. Yamamoto, *Nature (London)* **397**, 500 (1999).
- [41] I. I. Smolyaninov, A. V. Zayats, A. Gungor, and C. C. Davis, *Phys. Rev. Lett.* **88**, 187402 (2002).
- [42] M. Bamba, A. Imamoğlu, I. Carusotto, and C. Ciuti, *Phys. Rev. A* **83**, 021802(R) (2011).
- [43] T. C. H. Liew and V. Savona, *Phys. Rev. Lett.* **104**, 183601 (2010).
- [44] A. Miranowicz, M. Paprzycka, Y.-X. Liu, J. Bajer, and F. Nori, *Phys. Rev. A* **87**, 023809 (2013).
- [45] P. Rabl, *Phys. Rev. Lett.* **107**, 063601 (2011).
- [46] J.-Q. Liao and C. K. Law, *Phys. Rev. A* **82**, 053836 (2010).
- [47] P. Kómár, S. D. Bennett, K. Stannigel, S. J. M. Habraken, P. Rabl, P. Zoller, and M. D. Lukin, *Phys. Rev. A* **87**, 013839 (2013).
- [48] J.-Q. Liao and F. Nori, *Phys. Rev. A* **88**, 023853 (2013).
- [49] A. J. Hoffman, S. J. Srinivasan, S. Schmidt, L. Spietz, J. Aumentado, H. E. Türeci, and A. A. Houck, *Phys. Rev. Lett.* **107**, 053602 (2011).
- [50] C. Lang, D. Bozyigit, C. Eichler, L. Steffen, J. M. Fink, A. A. Abdumalikov, Jr., M. Baur, S. Filipp, M. P. da Silva, A. Blais, and A. Wallraff, *Phys. Rev. Lett.* **106**, 243601 (2011).
- [51] R. W. Boyd, *Nonlinear Optics* (Academic Press, New York, 2008).
- [52] M. J. Collett and C. W. Gardiner, *Phys. Rev. A* **30**, 1386 (1984).
- [53] C. W. Gardiner and M. J. Collett, *Phys. Rev. A* **31**, 3761 (1985).
- [54] H. Z. Shen, M. Qin, and X. X. Yi, *Phys. Rev. A* **88**, 033835 (2013).
- [55] A. Verger, C. Ciuti, and I. Carusotto, *Phys. Rev. B* **73**, 193306 (2006).
- [56] R. Loudon, *The Quantum Theory of Light* (Oxford University Press, Oxford, 2003).
- [57] S. Ferretti and D. Gerace, *Phys. Rev. B* **85**, 033303 (2012).
- [58] H. J. Carmichael, R. J. Brecha, and P. R. Rice, *Opt. Commun.* **82**, 73 (1991).
- [59] S. Weis, R. Rivi' ere, S. Del eglise, E. Gavartin, O. Arcizet, A. Schliesser, and T. J. Kippenberg, *Science* **330**, 1520 (2010).
- [60] M. D. Lukin, *Rev. Mod. Phys.* **75**, 457 (2003).
- [61] S. Ferretti, L. C. Andreani, H. E. Treci, and D. Gerace, *Phys. Rev. A* **82**, 013841 (2010).